DOI: 10.13009/EUCASS2019-352

Laminar to Turbulent Transition with Transport Equation on 2D and 3D Incompressible Flows

Donato de Rosa⋆† *and Pietro Catalano*⋆
⋆*CIRA - Italian Aerospace Research Centre*
Via Maiorise, Capua, Italy
d.derosa@cira.it · p.catalano@cira.it
†Corresponding author

Keywords: Transition, Intermittency, RANS, LES, Incompressible

1. Introduction

The prediction of boundary-layer transition region plays a key role in the simulation of aerodynamic flows in order to correctly predict lift and drag forces and, thus, the overall performance. The design of airfoils and wings is strongly affected by the accuracy in transition prediction. This requirement is further stressed for all the cases where the laminar-turbulent transition process highly influences the flow field, such as natural laminar-flow, laminar flow control, rotor helicopter and wind turbine blade design.

Reynolds Averaged Navier Stokes (RANS) equations are widely used by the aeronautical industry for the simulation of viscous flows, and CFD codes' capabilities in simulating fully turbulent flows have been widely assessed. Several attempts to improve the reliability of numerical results were performed in order to reproduce free transitional flows. An usual way is to impose a transition point in 2D and a line in 3D environment. This technique requires *a priori* knowledge of the transition location from experimental data or the use of other transition prediction approaches like engineering correlations or e^N method.[1,2] Nevertheless, transition region is not computed in CFD codes and a sudden shift between laminar and turbulent region is observed. Hence, in the last decades, several methods to model the transition region have been investigated. Some of these models are based on a physics-based RANS formulation and the most prominent is the Laminar Kinetic Energy proposed by Walters and Leylek.[3,4] Recently, a new correction was also proposed by Lopez and Walters.[5] An alternative to physics-based formulation is the so-called Local-Correlation based Transition Modeling (LCTM) concept, where the different transition processes are not modeled, but a set of transport equations are formulated to combine experimental correlations via triggering functions. A widely known model is the one proposed by Langtry and Menter,[6] namely the $\gamma - Re_\theta$ model. In 2015, Menter et al.[7] proposed a new transition model, namely the γ model, that is based on the previous one, but only the transport equation for the intermittency is present while the momentum-thickness Reynolds number is algebraically computed using local variables. In addition to a simplified formulation for the momentum-thickness Reynolds number, this model is also Galilean invariant, unlike the previous one. This paper deals with the implementation of the γ model[7] coupled with the $\kappa - \omega$ SST turbulence model, into the in-house RANS flow solver UZEN[8] and its validation for 2D and 3D flows.

For bi-dimensional analyses the Eppler 387 airfoil[9] is used. Results from RANS code are compared with experimental data and Large Eddy Simulation (LES) results. A low Reynolds number airfoil, namely SD 7003, is also simulated and compared with LES results.[10,11] The 6 : 1 prolate spheroid[12] is used as three-dimensional test case, where transition process is induced by both Tollmien-Schilchting and cross-flow instabilities.

2. Theoretical formulation

The transition model[7] is composed of the intermittency transport equation which is defined as follows:

$$\frac{\partial \rho\gamma}{\partial t} + \frac{\partial \rho U_j \gamma}{\partial x_j} = P_\gamma - D_\gamma + \frac{\partial}{\partial x_j}\left[\left(\mu + \frac{\mu_t}{\sigma_\gamma}\right)\frac{\partial \gamma}{\partial x_j}\right] \tag{1}$$

where γ, ρ and μ are the intermittency function, the density and the dynamic viscosity, respectively. x_j and U_j are the coordinates and velocity components for $j = 1 \ldots 3$. The transition source term P_γ and the destruction/relaminarization term D_γ are defined as:

$$P_\gamma = F_{length}\rho S \gamma(1-\gamma)F_{onset} \tag{2}$$

DOI: 10.13009/EUCASS2019-352

$$D_\gamma = c_{a2}\rho\Omega\gamma F_{turb}(c_{e2}\gamma - 1) \tag{3}$$

where S is the strain rate magnitude and Ω is the magnitude of the absolute vorticity rate. The constants in equations 1 2 and 3 are reported in table 1.

F_{length}	c_{e2}	c_{a2}	σ_γ
100	50	0.06	1.0

Table 1: γ model constants

Transition onset is controlled by the triggering functions F_{onset} and F_{turb}, not reported for sake of simplicity. In the current model, conversely to the $\gamma - Re_\theta$[6,13] there is no transport equation for the transitional Reynolds number Re_{θ_t}, used to compute the critical Reynolds number Re_{θ_c}, but an algebraic formula was developed:

$$Re_{\theta_c}(Tu_L, \lambda_{\theta L}) = C_{TU1} + C_{TU2}\exp\left[-C_{TU3}Tu_L F_{PG}(\lambda_{\theta L})\right] \tag{4}$$

2.1 Turbulence Model Coupling

Transition model is coupled with the standard $\kappa - \omega$ SST turbulence model.[14] The formulation considers to modify the transport equation for turbulent kinetic energy κ:

$$\frac{\partial}{\partial t}(\rho k) + \frac{\partial}{\partial x_j}(\rho u_j k) = \tilde{P}_k + P_k^{lim} - \tilde{D}_k + \frac{\partial}{\partial x_j}\left((\mu + \sigma_k\mu_t)\frac{\partial k}{\partial x_j}\right) \tag{5}$$

$$\tilde{P}_k = \gamma P_k \tag{6}$$

$$\tilde{D}_k = max(\gamma, 0.1)D_k \tag{7}$$

$$\mu_t = \rho\frac{a_1 k}{max(a_1\omega, F_2 S)} \tag{8}$$

where P_k and D_k are the production and destruction terms from the turbulent kinetic energy equation in the original SST turbulence model and P_k^{lim} is an additional production term:

$$P_k^{lim} = 5C_k max(\gamma - 0.2, 0)(1 - \gamma)F_{on}^{lim} max(3C_{SEP}\mu - \mu_t, 0)S\Omega \tag{9}$$

$$F_{on}^{lim} = min(max(\frac{Re_V}{2.2Re_{\theta_c}^{lim}} - 1, 0), 3) \tag{10}$$

$$Re_{\theta_c}^{lim} = 1100 \quad C_k = 1.0 \quad C_{SEP} = 1.0 \tag{11}$$

The transport equation for turbulent dissipation ω is kept as in the original formulation, instead.

2.2 Cross-flow correction

Original version of the γ transition model did not take into account for the cross-flow induced transition. Recently, a correction has been proposed.[15] This introduces a local formulation in the functional form:

$$T_{C1\ local} = \frac{C_{RSF}}{150}(G\Psi Re_v) > 1 \tag{12}$$

The function G accounts for the influence of pressure gradient, the function Ψ accounts for the ratio of the cross-flow strength relative to the streamwise strength and the Reynolds number effect is included through Re_v. The correlation can be adjusted by the constant C_{RSF}. The cross-flow indicator function Ψ is defined as follows:

$$\Psi = \left|\vec{\phi}\right| d_w \tag{13}$$

where ϕ is the dot product of the wall normal versor with the gradient of vorticity versor

$$\vec{\phi} = \vec{n} \cdot \nabla\vec{e}_\omega \qquad \vec{e}_\omega = \frac{\vec{\Omega}}{|\Omega|} \tag{14}$$

and d_w is the distance from the wall.

DOI: 10.13009/EUCASS2019-352

The triggering function that accounts for the cross-flow effects is defined as follows:

$$F_{onset,CF} = min[max\left[100(T_{C1\ local} - 1), 0\right], 1] \tag{15}$$

The source term in the equation 5 is then triggered, either by the primary triggering function F_{onset}, or by $F_{onset,CF}$.

$$F_{onset} = max(F_{onset}, F_{onset,CF}) \tag{16}$$

This upgraded formulation, above summarized, has been implemented in the in-house developed solver.

3. Numerical algorithm

The transport eq. 1 can be written in integral form, by applying the Gauss theorem, as:

$$\frac{d}{dt}\int_{\Omega}\rho\gamma d\Omega + \int_{\partial\Omega}\left[\rho\vec{v}\gamma - \left(\mu + \frac{\mu_t}{\sigma_\gamma}\right)\nabla\gamma\right]\cdot\vec{n}dS = \int_{\Omega}\left(P_\gamma - D_\gamma\right)d\Omega \tag{17}$$

where Ω is the computational domain and $\partial\Omega$ is its boundary surface.

For each computational cell (i, j, k), the previous equation becomes:

$$\frac{d}{dt}\int_{\Omega_{ijk}} U_{ijk}d\Omega_{ijk} + \int_{\partial\Omega_{ijk}}\left(F^c - F^v\right)dS_{ijk} = \int_{\Omega_{ijk}} Qd\Omega_{ijk} \tag{18}$$

where U is the vector of unknown $\rho\gamma$, F^c and F^v are the convective and dissipative fluxes, respectively, and Q is the source term.

By means of cell centered finite volume approach, the eq. 18 reduces to:

$$\Omega_{ijk}\frac{dU_{ijk}}{dt} + R^c_{ijk} - R^v_{ijk} - \Omega_{ijk}Q_{ijk} = 0 \tag{19}$$

with R^c_{ijk} and R^v_{ijk} the total net convective and dissipative fluxes positive if outgoing from the total volume Ω_{ijk}.

3.1 Convective fluxes

The residual R^c_{ijk} is obtained as the sum of the fluxes across the six faces of the cell (i, j, k). The flux $f_{i+1/2}$ at the interface $i + 1/2$ of the cell (i, j, k) is evaluated, by using a first order upwind scheme, as:

$$f_{i+1/2} = \frac{1}{2}\left[V_n\left(U_{i+1} - U_i\right) - |V_n|\left(U_{i+1} - U_i\right)\right] \tag{20}$$

with V_n the mean velocity normal to the interface.

3.2 Dissipative fluxes

The residual R^v_{ijk} is obtained as the sum of the fluxes across the six faces of the cell (i, j, k).The flux $g_{i+1/2}$ at the interface $i + 1/2$ of the cell (i, j, k) is evaluated as:

$$g_{i+1/2} = (\mu_{tot})_{i+1/2}\left(\nabla_i U\right)_{i+1/2} \tag{21}$$

The total viscosity coefficient is computed performing an average of the values μ and μ_t at the cells sharing the considered interface, while the i component of the gradient of the unknown vector U is evaluated as:

$$\left(\nabla_i U\right)_{i+1/2} = \frac{U_{i+1} - U_i}{\Delta n_{i+1/2}} \qquad \Delta n_{i+1/2} = \frac{\Omega_{i+1} + \Omega_i}{2A_{i+1/2}} \tag{22}$$

with $A_{i+1/2}$ the area **vector** of the face $(i + 1/2, j, k)$, and Ω_i the volume of the cell (i, j, k).

DOI: 10.13009/EUCASS2019-352

3.3 Source terms

The production of γ is computed as:

$$P_\gamma = F_{length}\gamma\left(1-\frac{\gamma}{\rho}\right)F_{onset}\sqrt{2A_1+A_2+A_3+A_4} \tag{23}$$

where

$$A_1 = \left(\frac{\partial u}{\partial x}\right)^2 + \left(\frac{\partial v}{\partial y}\right)^2 + \left(\frac{\partial w}{\partial z}\right)^2; \quad A_2 = \left(\frac{\partial u}{\partial y}+\frac{\partial v}{\partial x}\right)^2$$
$$A_3 = \left(\frac{\partial u}{\partial z}+\frac{\partial w}{\partial x}\right)^2 \quad A_4 = \left(\frac{\partial w}{\partial y}+\frac{\partial v}{\partial z}\right)^2$$

The destruction term is computed as:

$$D_\gamma = c_{a2}F_{turb}\gamma\left(c_{e2}\frac{\gamma}{\rho}-1\right)\sqrt{B_1+B_2+B_3} \tag{24}$$

where

$$B_1 = \left(\frac{\partial w}{\partial y}-\frac{\partial v}{\partial z}\right)^2 \quad B_2 = \left(\frac{\partial u}{\partial z}-\frac{\partial w}{\partial x}\right)^2 \quad B_3 = \left(\frac{\partial v}{\partial x}-\frac{\partial u}{\partial y}\right)^2$$

4. Eppler 387 airfoil

Low-Reynolds number airfoils are used in applications such as remotely-piloted vehicles, wind turbines, ultra-light aircraft and propellers. One of the difficulties associated with such airfoils is the presence of separated flow regions on the upper surface, which are inadequately modeled in the commonly used airfoil design and analysis codes.

The Eppler 387 (E387) is a low-Reynolds number airfoil which harbors a separation bubble at various angles of attack as fully documented by McGhee.[9] Current analyses were performed at a Reynolds number of $Re = 3\times10^5$ in incompressible regime, with a range of angles of attack of $\alpha = [0^\circ : 7^\circ]$. Freestream turbulence is set at $Tu = 1\%$ and eddy viscosity ratio at $\frac{\mu_t}{\mu} = 0.03$. Large Eddy Simulation (LES) was also carried out for the two angles of attack $\alpha = 1^\circ$ and 7°. Firstly, RANS simulations were performed using five different grid sizes at $\alpha = 1^\circ$ and $\alpha = 7^\circ$. Table 2 reports the number of cells and points for each grid, as well as the number of points on the airfoil surface.

	Grid 1	Grid 2	Grid 3	Grid 4	Grid 5
Number of cells	64000	100000	144000	196000	256000
Number of points	131788	204728	293668	398608	519548
Number of points on airfoil	481	601	721	841	961

Table 2: RANS grid dimensions

Figure 1 shows the distribution of y^+. The value is lower than 0.2 for the "coarse" grid already, below the suggested value.[7]

DOI: 10.13009/EUCASS2019-352

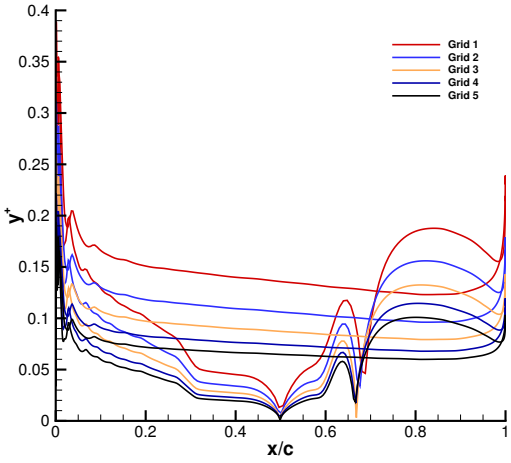

Figure 1: E387 - Dimensionless wall distance y^+

Figure 2 shows the comparison of experimental pressure coefficient distribution with the solution of RANS simulations on the five grids. The increase of the number of points on the airfoil surface leads to an improvement of the solution, in particular, in the bubble region. The match with experimental data at $\alpha = 1°$ is satisfactory as shown in figure 2(a), and the bubble location is well predicted. At $\alpha = 7°$, shown in figure 2(b), a bubble not visible in experimental data is numerically predicted on the upper side for all the grids.

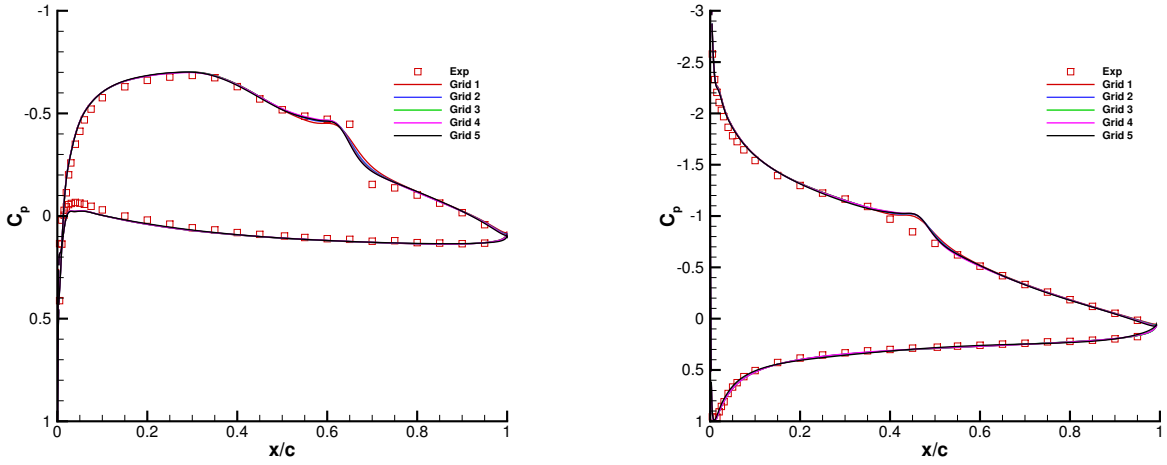

(a) $\alpha = 1°$ (b) $\alpha = 7°$

Figure 2: E387 - Pressure coefficient, RANS

The effect of grid refining is most appreciable in terms of skin friction coefficient, shown in figure 3. Laminar region is mostly unaffected, while the recovery in turbulent region is steeper increasing the number of points with higher skin friction coefficient values.

Lift and drag coefficients computed on the five grids are reported in tables 3 and 4 at $\alpha = 1°$ and $7°$, respectively. The comparison with experimental data shows an improvement of the solution with grid refinement.

	Experimental	Grid 1	Grid 2	Grid 3	Grid 4	Grid 5
C_l	0.465	0.492	0.491	0.490	0.489	0.488
C_d	0.0093	0.00897	0.00890	0.00886	0.00879	0.00878

Table 3: E387 - Lift and drag coefficients at $\alpha = 1°$

DOI: 10.13009/EUCASS2019-352

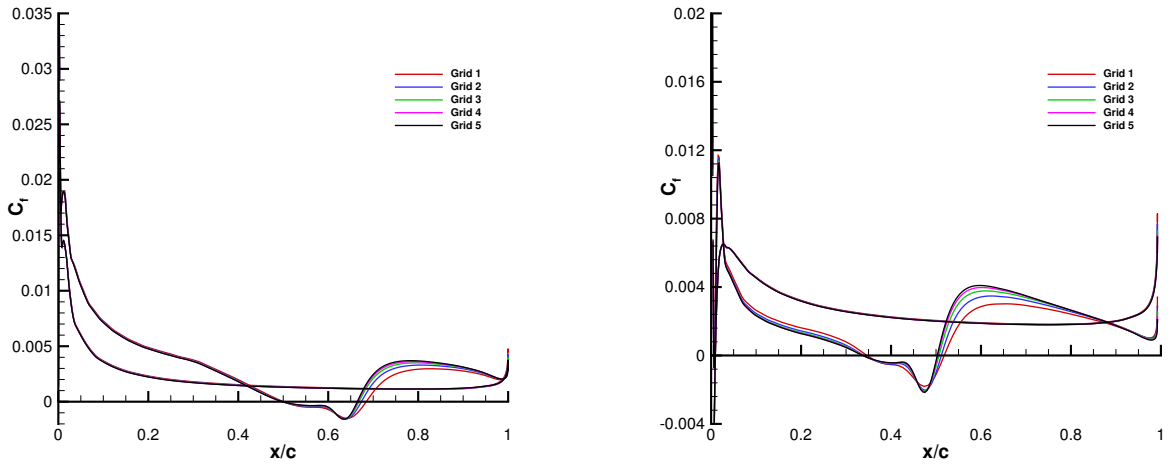

(a) $\alpha = 1°$ (b) $\alpha = 7°$

Figure 3: E387 - Skin friction coefficient, RANS

	Experimental	Grid 1	Grid 2	Grid 3	Grid 4	Grid 5
C_l	1.106	1.143	1.140	1.139	1.137	1.134
C_d	0.0129	0.0146	0.0144	0.0142	0.0141	0.0137

Table 4: E387 - Lift and drag coefficients at $\alpha = 7°$

Simulations at other angles of attack were also performed using the finest grid, and results in terms of global coefficients are presented in figure 4(a) for lift and figure 4(b) for polar curve. A shift in terms of lift coefficient is present, but a good agreement with experimental data is achieved. The drag coefficient is in accordance with experimental values for low angles of attack, while at high angles of attack a difference up to 20 drag counts is observed. Nevertheless, this discrepancy is likely due to the numerically predicted bubble, and a tuning of the model could further improve the results.

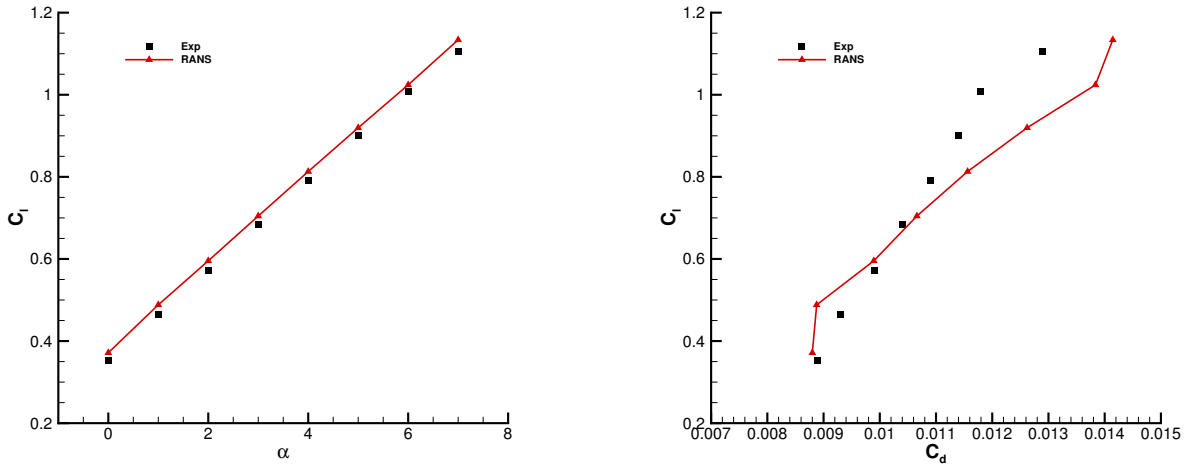

(a) Lift coefficient curve (b) $C_l - C_d$

Figure 4: Experimental - numerical comparison global coefficients

For the Large Eddy Simulations an appropriate C-Grid mesh of 1328 cells along wake and airfoil surface was built. In normal direction, the number of cells is 192, while in spanwise direction 96 cells were used. The spanwise

DOI: 10.13009/EUCASS2019-352

length was 10% of airfoil chord. The plus coordinates on the airfoil are shown in figure 5.

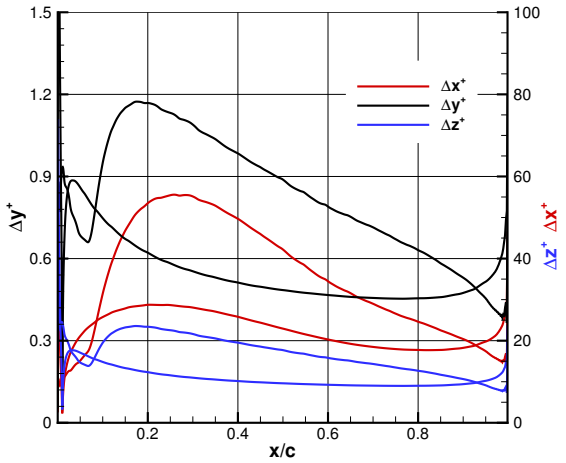

Figure 5: LES coordinates in plus unit

Pressure coefficient distribution obtained by LES is, then, compared with experimental data and RANS simulations on the finest grid. The results obtained with LES match better the experimental data at both angles of attack as shown in figure 6. In addition, a comparison in terms of skin friction is also performed. Figure 7(a) refers to $\alpha = 1°$ and it can be seen that laminar regions computed by RANS and LES are in good agreement, while the modeling of the bubble differs. In detail, LES recovers steeply in the turbulent region of the bubble with higher turbulent skin friction values. A transition to turbulent flow is observed at $x/c \approx 10\%$ on the upper side of the airfoil at $\alpha = 7°$ in the LES solution, as shown in figure 7(a). Transition prevents the bubble leading to a more accurate pressure coefficient distribution.

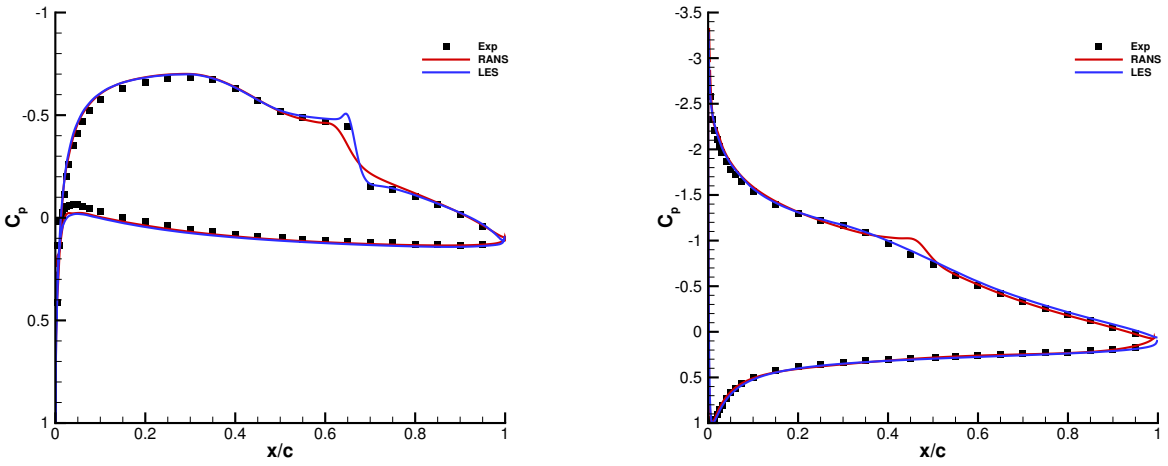

(a) $\alpha = 1°$ (b) $\alpha = 7°$

Figure 6: E387 - Pressure coefficient, LES

DOI: 10.13009/EUCASS2019-352

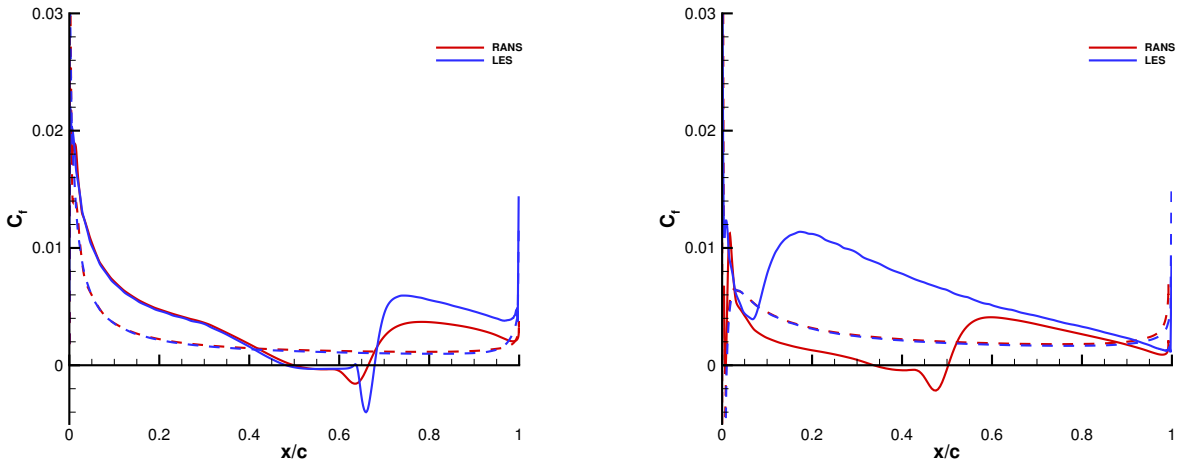

(a) $\alpha = 1°$ (b) $\alpha = 7°$

Figure 7: E387 - Skin friction coefficient, LES. Solid line: upper side; dashed line: lower side

5. SD 7003 airfoil

The Selig-Donovan (SD) 7003 airfoil, as Eppler 387, exhibits a laminar separation bubble over a wide range of incidences. Both RANS and LES[11] analyses were performed at $\alpha = 4°$ and $Re = 6 \times 10^4$ and a comparison is presented. The grid size for LES is 768 cells for airfoil and wake, 176 cells in normal direction, and 48 cells in spanwise direction. Pressure coefficient distribution is compared in figure 8, where LES exhibits a steeper recovery in the bubble reattachment region as highlighted in the previous results. A higher expansion on the leading edge region is also observed with reference to RANS solution.

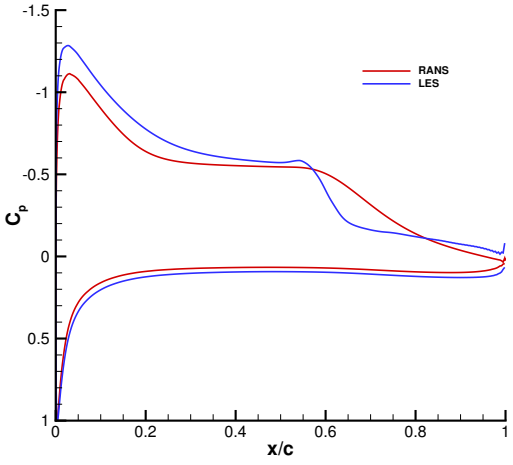

Figure 8: SD 7003 - Pressure coefficient

The different behaviour in the pressure recovery can be detailed by the comparison of skin friction distribution in figure 9. It is observed that LES predicts the reattachment point at $x/c \approx 63\%$ with a typical turbulent profile, while bubble simulated with RANS reattaches far downstream at $x/c \approx 86\%$. For this simulation, the γ model foresees the laminar separation bubble, but a low value of "turbulence" is produced, delaying the reattachment point and, hence, affecting pressure coefficient distribution.

DOI: 10.13009/EUCASS2019-352

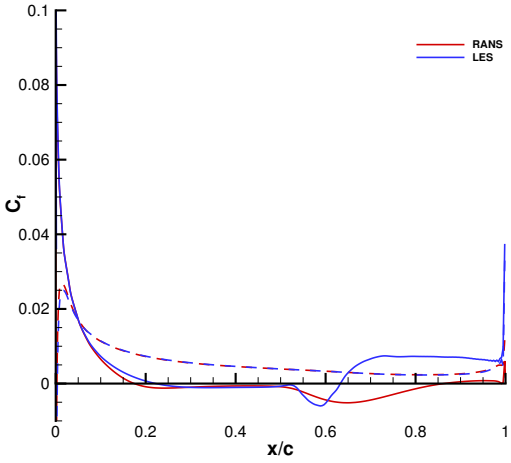

Figure 9: SD 7003 - Skin friction coefficient. Solid line: upper side; dashed line: lower side

The transition model provides a delayed reattachment point with reference to LES, but represents an improvement with respect to the standard SST model.[16]

6. 6:1 Prolate spheroid

Preliminary versions of transition models were validated for flows characterized by Tollmienn-Schlichting instability (TS) and by-pass mechanism, neglecting Cross-Flow waves (CF). For bi-dimensional flow field, models act correctly as CF instability is not present, but for three-dimensional configurations a non-negligible error can be observed. Several extensions for cross-flow instabilities were proposed for the $\gamma - Re_\theta$ model.[17–20] These extensions are based on the local helicity approach, adding a new set of correlations driven by helicity Reynolds number Re_{He}, yielding reasonable results. The previous approach is not extended to the one-equation transition model, but a cross-flow indicator function is introduced,[15] as briefly described above.

A widely used test case for transition prediction in three-dimensional analyses is the 6:1 inclined prolate spheroid. Experiments on this configuration were conducted in the low-speed tunnel at DLR by Kreplin et al.[21] For such configuration, transition occurs for CF instabilities. In order to assess the implemented modification, the simulations are performed at $\alpha = 15°$ and $Re = 6.50 \times 10^6$, with freestream turbulence and eddy viscosity ratio set at $Tu = 0.15\%$ and $\mu_t/\mu = 0.10$, respectively. Simulations are carried out on a structured grid made of 16 blocks and approximately 8×10^6 cells.

Cut-section plot of skin friction coefficient is performed. The cut-section plane is perpendicular to the 6:1 prolate-spheroid minor axis. Two sets of numerical results are presented, one relative to simulations without the cross-flow modification and the other one with the modification.

The results are shown in figure 10 and expose the fact that transition model without the correction for cross-flow predict transition downstream with reference to experimental data. The CF correction is able to predict transition onset near the experimental values although upstream. As a consequence, the transition zone shape is not correctly modeled and the predicted transition skin-friction coefficient peak value is lower than that of the experimental data.

Results are encouraging as the modification triggers the transition due to three-dimensional disturbances, nevertheless further investigations are demanded to better assess the model and to improve the solution.

7. Conclusions

The local correlation-based γ transition model for the prediction of laminar-turbulent transition, coupled with the $\kappa - \omega$ SST turbulence model, was implemented in the in-house CFD structured code. Results from the E387 airfoil showed a good agreement with the prediction of the bubble at $\alpha = 1°$, while a misleading result was obtained at $\alpha = 7°$. Lift and drag coefficients are in good agreement with experimental data in the analyzed range of angles of attack. LES results on the airfoil agrees with experimental data at both angles of attack. In detail, the pressure recovery is steeper with reference to RANS at $\alpha = 1°$, improving the match. At $\alpha = 7°$ a transition at $x/c \approx 10\%$ is predicted by LES, preventing the bubble, conversely to RANS. The numerical comparison with LES on the SD7003 airfoil presents a

DOI: 10.13009/EUCASS2019-352

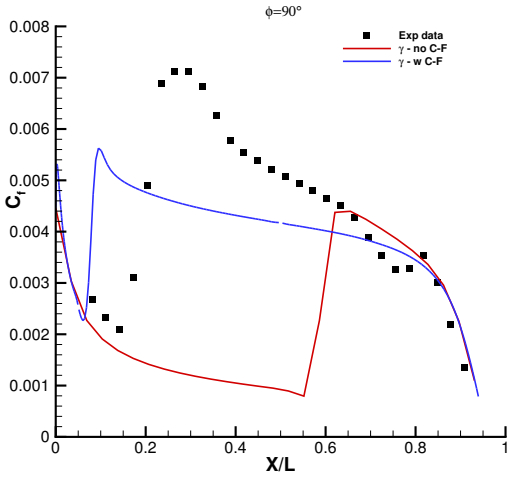

Figure 10: 6:1 prolate spheroid, skin friction coefficient

delayed reattachment point, but still an improvement with reference to more classical approaches. The rather low Reynolds number could be an issue for the transition model to investigate. The 6:1 inclined prolate spheroid was used to test the implementation of the C-F model. Preliminary results showed an improvement in the prediction of transition onset, but further analyses are required.

A more complete set of test cases, both bi-dimensional and three-dimensional, has to be investigated, in order to correct and assess the implementation. LES results should also be used to improve triggering correlation, especially.

References

[1] J. L. Van Ingen. A suggested semi–empirical method for the calculation of the boundary layer transition region. Technical Report VTH-74, University of Technology, Delft, 1956.

[2] J. van Ingen. The eN Method for Transition Prediction. Historical Review of Work at TU Delft. In *38th Fluid Dynamics Conference and Exhibit*, Reston, Virigina, jun 2008. American Institute of Aeronautics and Astronautics.

[3] D. Keith Walters and James H. Leylek. A new model for boundary layer transition using a single-point rans approach. *Journal of Turbomachinery*, 126(1):193–202, Mar 2004.

[4] D. Keith Walters and James H. Leylek. Computational fluid dynamics study of wake-induced transition on a compressor-like flat plate. *Journal of Turbomachinery*, 127(1):52–63, Feb 2005.

[5] Maurin Lopez and D. Keith Walters. A recommended correction to the k_t - k_l - ω transition-sensitive eddy-viscosity model. *Journal of Fluids Engineering*, 139(2):024501, dec 2016.

[6] Robin Langtry and Florian Menter. Transition modeling for general CFD applications in aeronautics. In *43rd AIAA Aerospace Sciences Meeting and Exhibit*. American Institute of Aeronautics and Astronautics (AIAA), jan 2005.

[7] Florian R. Menter, Pavel E. Smirnov, Tao Liu, and Ravikanth Avancha. A one-equation local correlation-based transition model. *Flow, Turbulence and Combustion*, 95(4):583–619, 2015.

[8] Pietro Catalano and Marcello Amato. An evaluation of RANS turbulence modelling for aerodynamic applications. *Aerospace Science and Technology*, 7(7):493–509, oct 2003.

[9] Robert J McGhee, Betty S Walker, and Betty F Millard. Experimental results for the Eppler 387 airfoil at low Reynolds numbers in the Langley low-turbulence pressure tunnel. 1988.

[10] P. Catalano, B. Mele, and R. Tognaccini. On the implementation of a turbulence model for low Reynolds number flows. *Computers and Fluids*, 109:67–71, March 2015.

[11] P. Catalano and R. Tognaccini. RANS analysis of the low-Reynolds number flow around the SD7003 airfoil. *Aerospace Science and Technology*, 15(8):615–626, dec 2011.

[12] H. P. Kreplin, H. Vollmers, and H. U. Meier. Wall shear stress measurements on an inclined prolate spheroid in the DFVLR 3m x 3m low speed wind tunnel, Göttingen. Technical report, DFVLR, 1985.

[13] Robin B. Langtry and Florian R. Menter. Correlation-based transition modeling for unstructured parallelized computational fluid dynamics codes. *AIAA Journal*, 47(12):2894–2906, Dec 2009.

[14] F. R. Menter. Two-equation eddy-viscosity turbulence models for engineering applications. *AIAA Journal*, 32(8):1598–1605, aug 1994.

[15] CFX Theory Guide.

[16] P. Catalano and R. Tognaccini. Turbulence Modeling for Low-Reynolds-Number Flows. *AIAA Journal*, 48(8):1673–1685, aug 2010.

[17] Cornelia Seyfert and Andreas Krumbein. Correlation-based transition transport modeling for three-dimensional aerodynamic configurations, 2012.

[18] Shivaji Medida and James Baeder. A new crossflow transition onset criterion for rans turbulence models, 2013.

[19] Cornelia Grabe and Andreas Krumbein. Extension of the $\gamma - re_{\theta t}$ model for prediction of crossflow transition. In *52nd Aerospace Sciences Meeting*. American Institute of Aeronautics and Astronautics (AIAA), jan 2014.

[20] Cornelia Grabe, Nie Shengyang, and Andreas Krumbein. Transition transport modeling for the prediction of crossflow transition, 2016.

[21] H.-P. Kreplin, H. Meier, and A. Maier. Wind tunnel model and measuring techniques for the investigation of three-dimensional turbulent boundary layers, 1978.